AIAA JOURNAL
Vol. 42, No. 3, March 2004

Mechanisms and Responses of a Single Dielectric Barrier Plasma Actuator: Geometric Effects

C. L. Enloe,* Thomas E. McLaughlin,† Robert D. VanDyken,‡ and K. D. Kachner§
U.S. Air Force Academy, Colorado Springs, Colorado 80840-6222
and
Eric J. Jumper,¶ Thomas C. Corke,** M. Post,†† and O. Haddad‡‡
University of Notre Dame, Notre Dame, Indiana 46556-5684

The single dielectric barrier discharge plasma, a plasma sustainable at atmospheric pressure, has shown considerable promise as a flow control device operating at modest (tens of watts) power levels. Measurements are presented of the development of the plasma during the course of the discharge cycle, and the relevance of these measurements to the modeling of the actuator's electrical properties is discussed. Experimental evidence is presented strongly pointing to the electric field enhancement near the leading edge of the actuator as a dominant factor determining the effectiveness of momentum coupling into the surrounding air. It is shown that the thrust produced by the actuator depends directly on the thickness of the exposed electrode even when the bulk discharge properties of the plasma remain unchanged. The case for field enhancement is bolstered by the application of an analytical model in closed form that, although an abstraction of the real actuator geometry, indicates that electric forces on charge imbalance in the plasma are concentrated predominantly near the edge of the exposed electrode. Both of these results are consistent with computational fluid dynamics calculations of the actuator in operation.

Introduction

THE dielectric barrier discharge is a type of plasma discharge with the unique property that it is self limiting and, therefore, sustainable at atmospheric pressures. Because of its usefulness in industrial applications, this type of discharge has been well studied.[1–14] The aerodynamic plasma actuator is a particular configuration of the dielectric barrier discharge, specifically, a surface discharge.[2,8]

Configuration of the Plasma Actuator

The configuration of the plasma actuator is simple, consisting of one electrode exposed to the surrounding air and one electrode completely encapsulated by a dielectric material arranged in the highly asymmetric geometry shown in Fig. 1, to which a high (10–20-kV peak-to-peak) ac voltage (1–10 kHz) is applied. Typically, the plasma actuator's electrodes are long and thin and are arranged spanwise on an aerodynamic surface. For this work, we typically used a 0.08-mm-thick, 1.27-cm-wide insulated copper foil electrode covered with 0.3 mm of Kapton® polyimide insulation. We varied the dimensions of the exposed electrode, using wires up to 0.98 mm in diameter and copper foils 0.64 mm wide and between 0.08 and 0.64 mm thick. When the high ac voltage is applied, a plasma discharge appears on the insulator surface above the insulated electrode (as shown in Fig. 2), and directed momentum is coupled into the surrounding air.[15,16] The amount of momentum coupling is sufficient to have a substantial effect on the airflow over the surface in such applications as drag reduction and reattachment of separated flows.[17–25]

As Fig. 2 shows, there are large-scale spatial structures in the discharge, visible to the unaided eye, that appear to be tied to irregularities in the electrodes. These undoubtedly have an effect on the efficiency of the actuator, and we plan to address these in future work. In previous work,[15,16,26] however, we have shown that there is also considerable temporal and spatial structure in the plasma indistinguishable to the unaided eye and that this structure is consistent with the operation of the dielectric barrier discharge. The plasma is formed as the result of a series of discharges as electrons are transferred onto and off of the dielectric surface. (This mechanism is shown schematically in Fig. 3.) The buildup of charge on the dielectric surface is fundamentally the reason that the discharge is self-limiting and does not collapse into a constricted arc. (Based on their energies, one would expect the electrons to penetrate at most a few monolayers into the dielectric material. Because of the low conductivity of the dielectric, the electrons will remain at the location where they are deposited.) For modeling purposes, the dielectric surface that is covered with the immobile charges effectively acts as an electrode in addition to the two physical electrodes in the problem.

In operation, the plasma in the discharge sweeps along the surface of the dielectric on each half-cycle of the applied ac voltage. Figures 4 and 5 show the results of optical observations made on the discharge in which the field of view of a photomultiplier tube was limited at any time to a distance of 0.25 mm in the chordwise direction. We take the light emissions from the plasma actuator as a surrogate for plasma density, specifically, for the electron density n_e, which, for a quasi-neutral plasma, is also approximately equal to n_i, the ion density. Using light emission to infer plasma density assumes that the recombination time of the plasma is short compared to the timescale of the discharge, but this assumption is confirmed by the observations and is consistent with plasma lifetimes reported in the literature.[27] By scanning the photomultiplier tube (PMT) over the surface and taking data synchronized with the ac voltage, we are able to make a temporal map of the extent of the plasma in the chordwise direction, shown in complementary presentations in Figs. 4 and 5. The map shows that the discharge ignites near the edge of the exposed electrode and that the extent of the plasma in the chordwise direction increases in time until the discharge quenches, when the

Received 15 July 2003; revision received 6 October 2003; accepted for publication 7 October 2003.

*Professor, Department of Physics. Senior Member AIAA.
†Research Associate, Department of Aeronautics. Associate Fellow AIAA.
‡Research Assistant, Department of Aeronautics.
§Cadet First Class, Department of Physics.
¶Professor, Department of Aerospace and Mechanical Engineering. Fellow AIAA.
**Clark Chair Professor, Department of Aerospace and Mechanical Engineering. Associate Fellow AIAA.
††Ph.D. Candidate, Department of Aerospace and Mechanical Engineering. Student Member AIAA.
‡‡Visiting Scholar, Department of Aerospace and Mechanical Engineering.

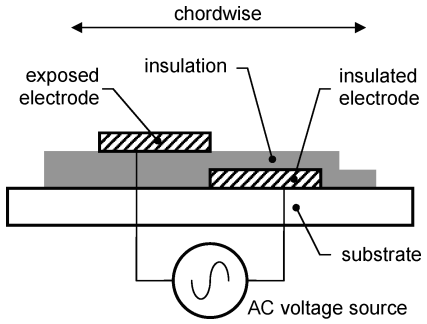

Fig. 1 Aerodynamic plasma actuator in a chordwise cross section.

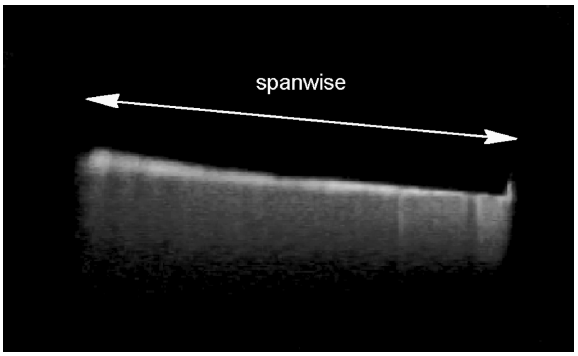

Fig. 2 Plasma actuator appears as a diffuse plasma formed on the surface of the dielectric above the insulated electrode.

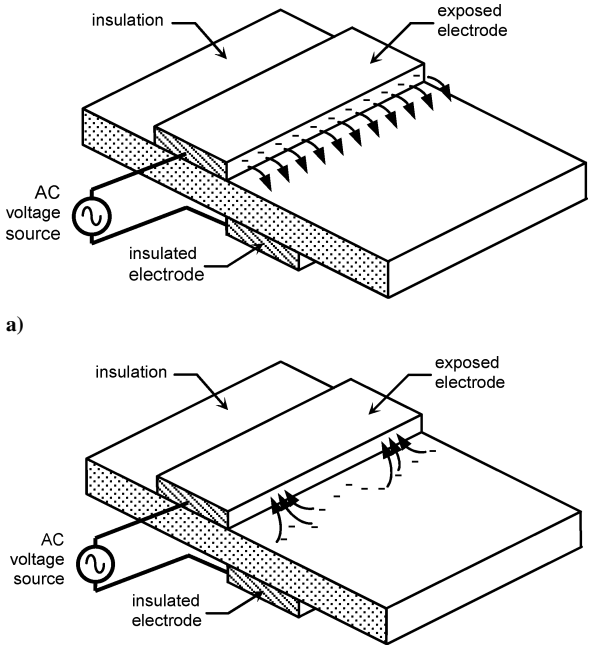

Fig. 3 Plasma actuator is a configuration of the dielectric barrier discharge, in which the discharge is self-limiting because electrons emitted from the exposed electrode collect on the dielectric surface, to be returned on the subsequent half-cycle of the discharge.

ac voltage reaches an extremum. Near the edge of the exposed electrode, the plasma density generally increases in time, although the relatively flat plateaus in the light emission for distances greater than 2 mm from the exposed electrode's edge indicate that density of the plasma sweeping over the surface is relatively uniform. As Fig. 5 shows, the rate at which the plasma sweeps over the dielectric surface (indicated by the slopes b and c of the wavefronts in Fig. 5) is the same for both the negative-going and positive-going half-cycles of the discharge. Consistent with the operation of the dielectric barrier

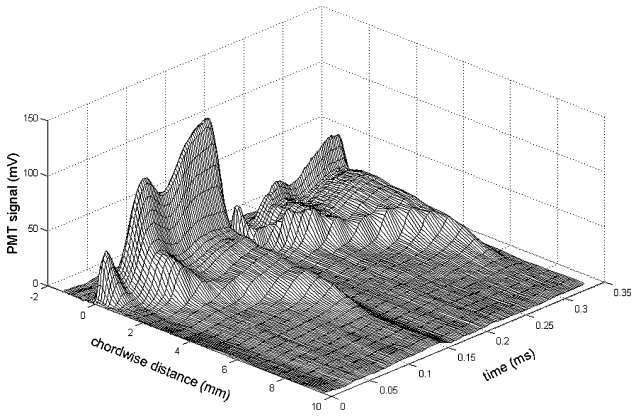

Fig. 4 Surface plot of light emission (proportional to plasma density) from the aerodynamic plasma actuator as a function of space and time, revealing substantial spatial and temporal structure.

discharge, it is necessary to maintain a changing voltage waveform with time to sustain the discharge; as shown at point a in Fig. 5, if the magnitude of dV/dt drops off even momentarily, the discharge starts to quench.

The rate at which the leading edge of the plasma expands over the dielectric surface, indicated by the slopes b and c in Fig. 5, depends on the amplitude and frequency of the applied voltage; for instance, at a given frequency, the plasma expands faster the greater the voltage amplitude applied to the circuit.[15,16]

Effects of Electrode Geometry on Actuator Effectiveness

Figure 5 shows the case of a plasma whose chordwise extent is limited by its rate of expansion and the frequency of the applied waveform. Not unexpectedly, we find that the expansion of the plasma is also limited by the extent of the lower, insulated electrode, that is, that the plasma will not expand more than a few millimeters past the downstream edge of the insulated electrode no matter how hard the circuit is driven because the strong electric field is limited to the region between the electrodes and does not extend downstream beyond the encapsulated electrode's edge. We find that this limitation on the plasma expansion also limits the effectiveness of the actuator.

Figure 6 shows the results of particle image velocimetry (PIV) measurements of the velocity induced in the air by the plasma actuator. Figure 6 shows a comparison of two different voltage amplitudes using different sizes of insulated electrodes. (Here, the electrodes are made of 0.025-mm-thick copper foil with 0.15-mm-thick Kapton polyimide used as the dielectric. The width of the exposed electrode is held constant at 12.7 mm.) As Fig. 6 shows, with 16 kV peak-to-peak applied in a triangular waveform, the velocity induced by the actuator increases with the increasing length of the insulated electrode. This is because for 16 kV applied, the length of this electrode limits the expansion of the plasma and, thus, the performance of the actuator. On the other hand, for a 12-kV peak-to-peak driving waveform, the air velocity attainable reaches an asymptotic maximum for an electrode length of approximately 12 mm. Increasing the width further has no effect on the actuator performance at this voltage level. In other words, the plasma cannot "use" more than 12 mm of chordwise length no matter the size of the lower electrode. This has practical implications for packing multiple actuators on an aerodynamic surface: It is useless, and a waste of space, to provide more insulated electrode width than can be covered by the plasma at the maximum anticipated applied voltage.

Because there are two physical electrodes that make up the plasma actuator, it is tempting to model the device as a capacitor driven by the ac voltage. In fact, however, because charge builds up on the dielectric surface and does not reach the insulated electrode, there are multiple capacitances in play in the circuit. Effectively, the top surface of the dielectric forms another electrode, and the simplest circuit model of the actuator (Fig. 7) must include this effective electrode in addition to the two physical electrodes.[15,16] Because, as

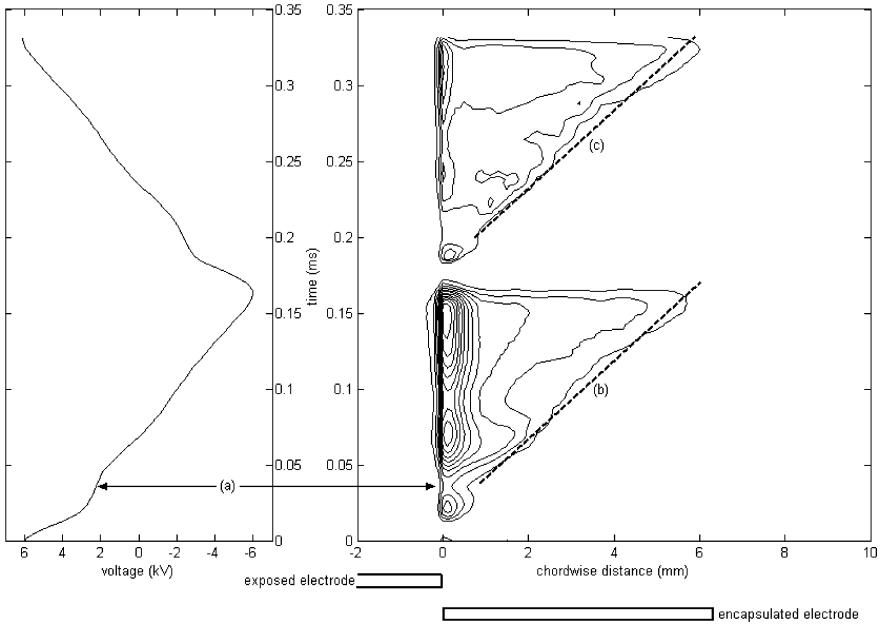

Fig. 5 Same data as Fig. 4 as contour map, simultaneous with the voltage waveform applied to the device: two distinct pulses of plasma per cycle of the applied voltage.

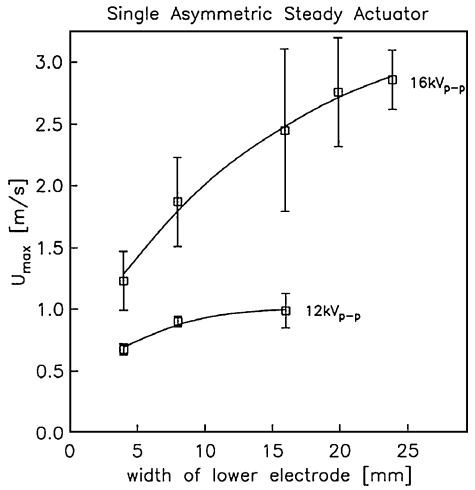

Fig. 6 Maximum velocity induced by the plasma actuator, for two different driving voltages, as a function of width of lower (insulated) electrode.

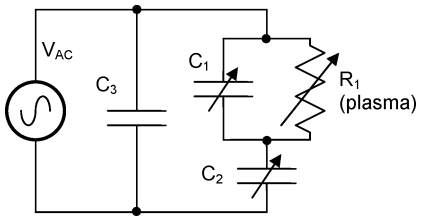

Fig. 7 Lumped-element circuit model of the plasma actuator takes into account the charging of the dielectric surface as an effective electrode.

indicated in Figs. 4 and 5, the area of the effective electrode changes in time, the capacitances that include this electrode must be treated as variable capacitances.

The capacitance C_3 in Fig. 7 represents the capacitance between the physical electrodes (exposed and insulated) in the system. This capacitance provides a path through which displacement current can flow in the circuit and, as such, does not have a direct effect on the discharge itself, although in practice any such reactive element in the circuit affects the complex impedance presented by the circuit to its driver and so has an effect on the shape of the applied voltage waveform.

The capacitance C_2, between the effective and insulated electrodes, is determined in part by the thickness of the dielectric used. As with C_3, it does not affect the voltage across the discharge directly; rather, it sets the voltage divider ratio on the right-hand leg of the circuit, which also includes the discharge itself. This has an important practical consequence: It is possible to make the actuator much less prone to electrical breakdown through the dielectric by making the dielectric thicker, without altering the electric field in the plasma (and reducing the performance of the actuator) if at the same time the input voltage waveform is adjusted to compensate for the change in the voltage divider ratio. The capacitance C_2varies in time, is small when the discharge ignites on each half-cycle of the applied voltage waveform, and increases as the plasma sweeps over the dielectric surface.

This is also true of the capacitance C_1, between the effective and exposed electrodes. In the circuit, C_1 is the key element because the potentials on its electrodes (both real and effective) set the boundary conditions for the plasma discharge and, hence, directly impact the performance of the actuator.

Because they vary as the discharge develops over the dielectric surface, the values of C_1 and C_2 are not under the direct control of the experimenter. Because of this, we decided to investigate other aspects of the effects of electrode geometry by changing the dimensions of the one electrode in the discharge path that we could control directly, the exposed electrode. As Figs. 4 and 5 show, the plasma extends downstream of the exposed electrode almost exclusively, so that the lateral extent of the exposed electrode is apparently immaterial to the discharge. Again, this is an aspect of the discharge with an immediate, practical consequence. As we show in Fig. 8, the effect of multiple actuators is additive if they are placed in reasonably close proximity: Two actuators placed one behind the other yield twice the velocity increase in the air as a single actuator, for a given applied voltage. (The degree to which this trend continues before reaching a limit is a subject for further investigations.) If the width of the exposed electrode can be made arbitrarily narrow, then the density with which multiple actuators can be placed chordwise along an aerodynamic surface can be maximized.

In contrast to the essentially negligible effect of the exposed electrode's width on the actuator performance, the thickness of this electrode has a profound effect on the actuator's efficiency. We

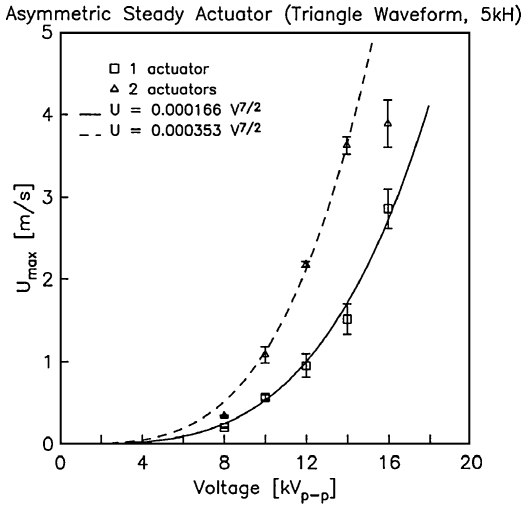

Fig. 8 Velocity increase of multiple actuators is additive: for given voltage, two actuators placed one behind the other give twice the velocity increase of single actuator alone; asymmetric steady actuator (triangle waveform, 5 kH).

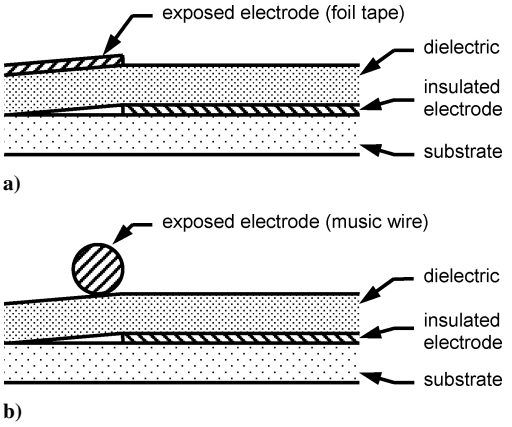

Fig. 9 Two sets of actuators: a) various thicknesses of metal foil tape as the exposed electrode and b) steel music wire as the exposed electrode.

developed two different, complementary sets of actuator electrodes to investigate the behavior of the actuator as we varied the electrode thickness. As shown in Fig. 9a, for one set of actuators, we use thin copper foil tape, 0.64 mm wide, to construct the upper, exposed electrodes. We layer the tape to vary the electrode thickness from 0.08 to 0.64 mm. For another set, we use steel music wire with a diameter ranging from 0.36 to 0.98 mm as the exposed electrode, as shown in Fig. 9b. The stiff steel wire was mechanically rigid and uniformly straight even in the smallest radius available to us. Although there is a difference in the effectively square cross section of the edge of the tape and the circular cross section of the wire, we felt that the Debye shielding in the plasma would largely wash out this difference, and our assumption turned out to be justified. We take half the thickness of the foil electrodes to be equivalent to the radius of the wire electrodes. For each of the cases shown here, the lower, insulated electrodes are identical: 1.27 mm wide, 0.08 mm thick, encapsulated by 0.3 mm of Kapton polyimide.

As we vary the thickness of the exposed electrode, we find that for a given ac voltage waveform, the gross structure of the plasma does not depend on the thickness or diameter of the exposed electrode. Figure 10 shows one measure of the bulk properties of the discharge, namely, power dissipation in the discharge as a function of voltage. We computed power by sampling the voltage and current waveforms for the entire circuit and numerically integrating the product of these waveforms over one period of the discharge, thus integrating out the reactive power and accounting exclusively for the power dissipated in the plasma. (We have shown that the functional relationship, approximately $P \propto V^{7/2}$, is typical for this surface dielectric barrier

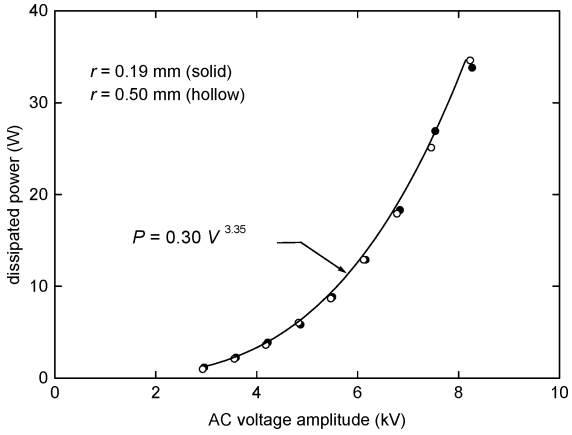

Fig. 10 Bulk properties of the plasma discharge do not depend on the geometry of the exposed wire electrode: solid and open symbols distinguish two electrode geometries.

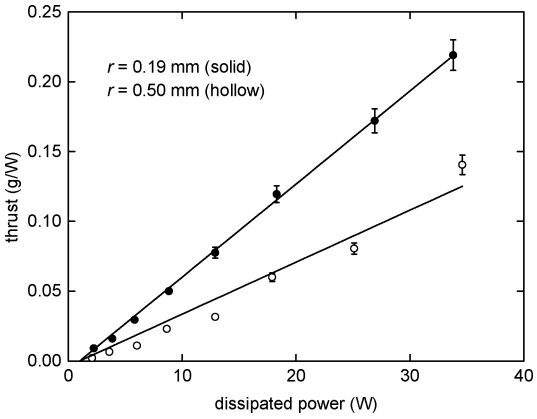

Fig. 11 Effectiveness of the plasma actuator strongly dependent on geometry of exposed wire electrode.

discharge.[15,16]) The voltage and current waveforms, not depicted here, show the same degree of similarity. Figure 10 specifically shows cases for two different wire radii overlaid, but the results are the same for all of the electrode configurations we tested: The bulk properties of the discharge are essentially identical for substantially different diameter exposed electrodes.

In dramatic contrast, however, the effectiveness of the actuator in coupling momentum into the air, as measured by the thrust produced by the actuator, depends strongly on the geometry of the exposed electrode. Figure 11 shows the thrust (measured directly with a mass balance) as a function of input power for two different radius wire electrodes, $r = 0.19$ and 0.50 mm. Both share a similar form: After the input power exceeds a threshold value of approximately 1 W, the thrust increases linearly with power, but the efficiency of the actuator in converting power to thrust is substantially greater with the thinner wire electrode. The trend is consistent not only with the radius of the wire electrodes, but with the dimensions of the foil tape electrodes as well. Figure 12 shows the thrust (in grams per watt) plotted against electrode dimension. The trend is clear: Although the bulk properties of the discharge remains unchanged, the thinner the exposed electrode, the greater the momentum transfer to the air is. For these tests, we did not measure the velocity profiles of the air directly; however, based on related measurements such as those shown in Figs. 6 and 8, we estimate a flow velocity on the order of 1–3 m/s in a millimeter-sized region above the actuator. This equates roughly to 1 mW or less of power in the airflow itself, or an overall efficiency on the order of 10^{-4} from a power standpoint. Fortunately, even this modest power input into the flow is dramatically effective in changing aerodynamic flow.[17–25]

We also note here that the functional relationship between dissipated power and input voltage amplitude is mirrored in the

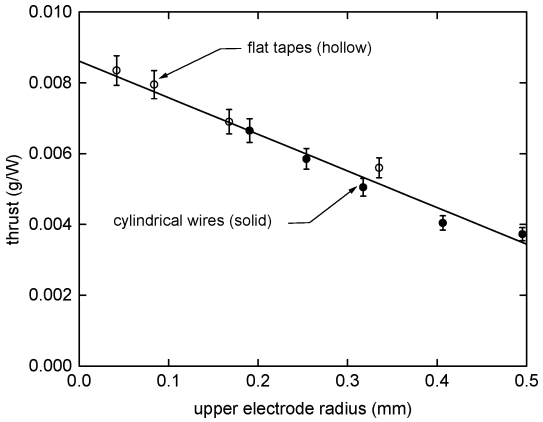

Fig. 12 Momentum transfer to air depends strongly on characteristic dimension of exposed electrode, even though this dimension does not affect bulk properties of the discharge.

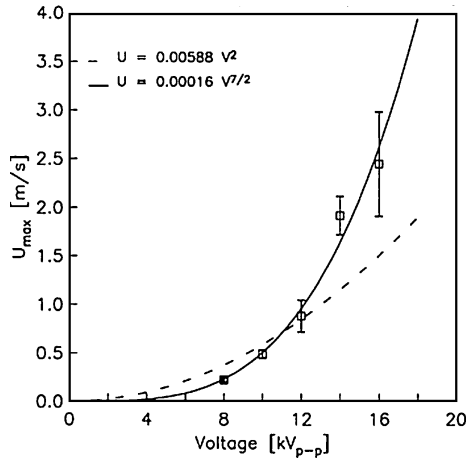

a) Single asymmetric steady actuator (square wave, 5 kH)

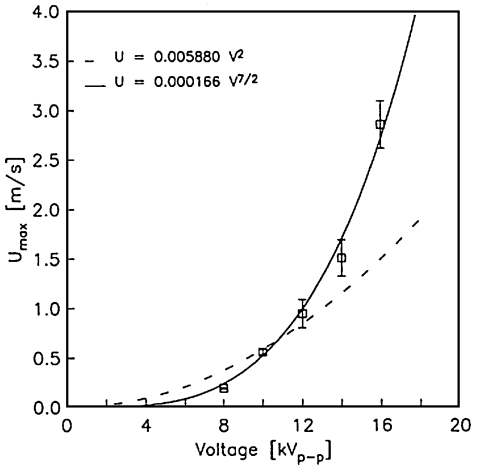

b) Single asymmetric steady actuator (triangle waveform, 5 kH)

Fig. 13 Maximum velocity induced in air by actuator approximately proportional to $V^{7/2}$; same proportionality as electrical power dissipated in actuator.

relationship between the maximum attainable velocity and the input voltage. Again, we use PIV techniques to measure the velocity induced in the air by the actuator and plot the maximum value we record in our PIV field of view vs the applied voltage amplitude. As Fig. 13 shows, irrespective of voltage waveform shape, the velocity imparted to the flow by the actuator goes approximately as $u_{\max} \propto V^{7/2}$, indicating a direct proportionality between the electrical power dissipated in the actuator and the velocity induced in the air. The efficiency of this coupling, however, appears to be controlled by interactions at the edge of the exposed electrode.

Electric Forces on the Plasma Actuator

The dimension of the exposed electrode does not affect the bulk discharge but substantially affects the performance of the actuator. This points to the well-established phenomenon of electric field enhancement near small electrode features[28] as a fundamental driver of actuator effectiveness. The case would be considerably strengthened if there were a sound theoretical basis for this concept. We can, indeed, establish this case by the use of an analytical model that, although an abstraction of the real actuator, nevertheless models the salient features of the device.

In evaluating the actuator's performance, we directly measure the thrust it produces with a mass balance: If we measure an apparent mass increase, it is because the actuator is pushing up on the other end of the arm. For us to be able to make this measurement, there must be a mechanical coupling between the moving air and the actuator. Because this coupling only occurs when the plasma is present, we can infer that the plasma is the intermediary. The way that the plasma can couple force into the actuator is via the electric field interactions with the charged particles in the plasma. Essentially, the charges in the plasma "push" on both the background gas and the image charges in the electrodes, which completes the chain of forces leading to a measurement of thrust.

Inasmuch as it has been created by the ionization of neutral air, the plasma will remain roughly electrically net neutral. If there is to be an interaction between the electric field and the plasma, this implies some type of local charge imbalance in the plasma due to the rearrangement of these equal positive and negative charges. Such an interaction, if it exists, can be analyzed by considering the collective behavior of the plasma.

Debye Shielding in Plasmas

To understand the operation of the plasma actuator, it is useful to understand how the plasma modifies the electric field that is otherwise present when the air between the electrodes is not ionized. (Without ionization, the relative dielectric constant of the air is effectively the same as that of a vacuum, $\varepsilon_r = 1$.) Although this treatment is accessible in any number of basic plasma physics texts,[29,30] it is useful to recap here because of what it implies about the behavior of the plasma. Because charges in a plasma are free to move, they arrange themselves to cancel as much of the field as possible within the plasma volume. Thermal motion of the particles causes this cancellation to be incomplete near the boundaries of the plasma. When a timescale long enough for the charges to redistribute themselves is assumed, we can relate the electron density n_e and the ion density n_i in the plasma to the local electric potential ϕ by the Boltzmann relation:

$$n_{i,e} = n_0 \exp[\mp(e\phi/kT_{i,e})] \approx n_0[1 \mp (e\phi/kT_{i,e})] \qquad (1)$$

where n_0 is the background plasma density, k is Boltzmann's constant, and T is the temperature of the particular species. In Eq. (1), the upper (minus) sign applies to the ions, whereas the lower (plus) sign applies to the electrons. The net charge density ρ at any point in the plasma is

$$\rho = e(n_i - n_e) \approx -en_0[(e\phi/kT_i) + (e\phi/kT_e)] \qquad (2)$$

From Maxwell's equations, and from the fact that the electric field $\boldsymbol{E}$ is related to the potential ϕ by $\boldsymbol{E} = -\nabla\phi$, we have

$$-\nabla^2\phi = \rho/\varepsilon_0 \qquad (3)$$

where ε_0 is the permittivity of free space. Using Eq. (3) in Eq. (2), we have

$$\nabla^2\phi = \left(e^2 n_0 \big/ \varepsilon_0\right)(1/kT_i + 1/kT_e)\phi = \left(1 \big/ \lambda_D^2\right)\phi \qquad (4)$$

where we have now defined the Debye length λ_D by

$$1 \big/ \lambda_D^2 = \left(e^2 n_0 \big/ \varepsilon_0\right)(1/kT_i + 1/kT_e) \qquad (5)$$

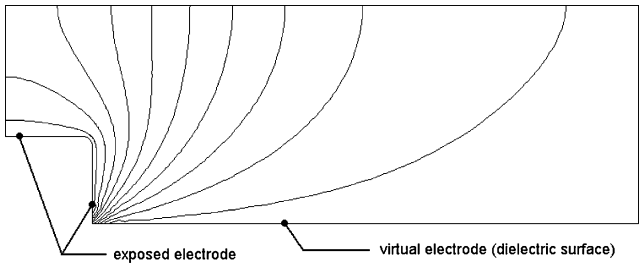

a)

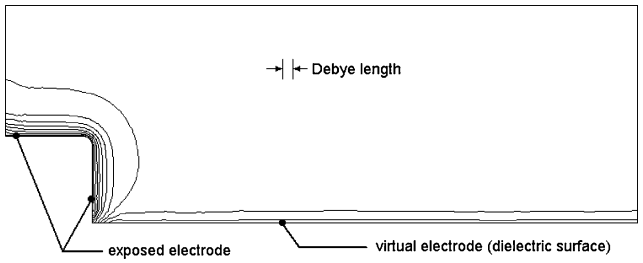

b)

Fig. 14 Electric potential for the plasma actuator electrode geometry calculated numerically a) without and b) with plasma case.

The Debye length is the characteristic length for electrostatic shielding in a plasma: For lengths greater than the order of λ_D, the plasma shields external potentials. Over dimensions on the order of λ_D in the vicinity of an exposed potential, the charge density in the plasma is imbalanced in favor of one of the species. Specifically, Eqs. (3) and (4) tell us that

$$\rho = -\left(\varepsilon_0 \big/ \lambda_D^2\right)\phi \tag{6}$$

or, in other words, that the net charge density at any point in the plasma is proportional to the potential at that point.

Electric Potential with Asymmetric Electrodes

Equation (4) can be solved numerically for any arbitrary geometry by applying finite element techniques. In Fig. 14, we show the solution to Eq. (4) for a model plasma actuator geometry, obtained using the finite element solver FEMLAB.[31,§§] In this geometry, the potentials are fixed at the surface of the exposed electrode (the lower left-hand corner of the simulation space) and at the surface of the dielectric barrier (the lower boundary of the simulation space), which effectively forms another electrode. In Fig. 14a we calculate a set of evenly spaced equipotentials in the absence of plasma by setting the Debye length to a very large value. In Fig. 14b, we include plasma (albeit of a uniform density throughout the simulation volume) by setting the Debye length small compared to the electrode dimensions, as shown. As predicted, Debye shielding effect limits the penetration of the potentials on the electrodes to a small region near the electrode surface.

Although it is very useful to be able to solve for Debye shielding in an arbitrary geometry, we could effectively parameterize our description of electric forces on the plasma if we could solve the problem in closed form. Unfortunately, Eq. (4) is generally not solvable in closed form except for a few special cases. For example, the simplest case, that of a slab of plasma between infinite plane parallel electrodes (the so-called one-dimensional plasma capacitor) is treated in many basic plasma textbooks.[29] Two other solvable cases are those of a plasma between nested, infinitely long concentric cylindrical electrodes and between nested, concentric spherical electrodes. Because of symmetry, both of these cases are solvable in terms of one radial dimension, r. Of these two, the former (shown in cross section in Fig. 15) is an acceptable abstraction of the plasma

[§§]Data available online at http://www.comsol.com [cited 4 April 2003].

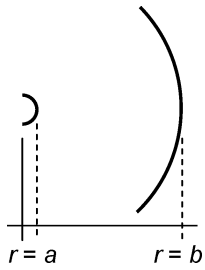

Fig. 15 Cylindrical plasma capacitor is an asymmetric electrode geometry amenable to closed-form solution.

actuator for our purposes. Like the real plasma actuator, it consists of electrodes that are substantially different in exposed area and that are long in their linear dimension compared to their cross-sectional dimensions. We know that there is a spatial structure to the electric field even in the absence of the plasma, which the presence of the plasma will enhance. Effectively, we have wrapped the plasma actuator into a mathematically tractable form. As such, we expect our abstract model to yield some insights about the behavior of the plasma in the real actuator geometry. The other advantage of cylindrical geometry is that the solution in the absence of the plasma is well known, and we can recover the infinite parallel plate geometry in the limit of large electrode radii compared to electrode spacing, so that we have several known points against which to test our solution.

Equation (4) in cylindrical geometry is

$$\frac{1}{r}\frac{\partial}{\partial r}\left(r\frac{\partial \phi}{\partial r}\right) = \frac{1}{\lambda_D^2}\phi \tag{7}$$

This is a boundary-value problem, and we set the boundary conditions such that the electric potential $\phi(r)$ is $\phi(a) = \phi_a$ at the radius of the inner electrode and $\phi(b) = \phi_b$ at the radius of the outer electrode. The solution is then a sum of the hyperbolic Bessel functions I_0 and K_0, given by

$$\phi(r) = C_1 I_0(r/\lambda_D) + C_2 K_0(r/\lambda_D) \tag{8}$$

where the constants C_1 and C_2, chosen to satisfy the boundary conditions are given by

$$C_1 = \left\{\phi_a - \phi_b\left[\frac{K_0(a/\lambda_D)}{K_0(b/\lambda_D)}\right]\right\} K_0\left(\frac{b}{\lambda_D}\right) \Bigg/ \left[I_0\left(\frac{a}{\lambda_D}\right)K_0\left(\frac{b}{\lambda_D}\right) - I_0\left(\frac{b}{\lambda_D}\right)K_0\left(\frac{a}{\lambda_D}\right)\right] \tag{9}$$

$$C_2 = \frac{\phi_b - C_1 I_0(b/\lambda_D)}{K_0(b/\lambda_D)} \tag{10}$$

Another condition on the solution is that the plasma maintain charge neutrality so that integrated over its volume V,

$$\int \rho \, \mathrm{d}V = 0 \tag{11}$$

(In other words, because the air was initially neutral before it was ionized, ionization creates no net electric charge.) When Eq. (6) is used in Eq. (11), the neutrality condition implies that

$$0 = -2\pi \frac{\varepsilon_0}{\lambda_D^2}\int_a^b r\phi(r)\,\mathrm{d}r \tag{12}$$

Applying this condition to the solution defined by Eqs. (8–10) yields, as the final condition,

$$0 = C_1 b I_1(b/\lambda_D) - C_1 a I_1(a/\lambda_D) - C_2 b K_1(b/\lambda_D) + C_2 a K_1(a/\lambda_D) \tag{13}$$

Equations (8–10) and (13), then, define the solution to Debye shielding in a cylindrical plasma capacitor. To gain confidence in the accuracy of this mathematical description, we can evaluate the solution

in several limiting cases to test its validity. As an example, we take the case in which we have the inner radius normalized and interelectrode gap much larger than the radius of the inner electrode, $a = 1$, $b - a = 10$. We also normalize the potential difference between the electrodes, so that $\phi_a - \phi_b = 1$. With the plasma present, we set the Debye length much shorter than the interelectrode gap, $\lambda_D = 1$. The requirements of charge neutrality, given in Eq. (13), lead us to set $\phi_a = 0.9$ and $\phi_b = -0.1$ for a normalized potential drop $\phi_a - \phi_b = 1$ between the electrodes. The solution is shown by the solid line in Fig. 16. The shielding properties of the plasma are evident: The potential in the plasma is zero except near the inner and outer boundaries.

To check the solution, we can "remove" the plasma by setting the Debye length in Eqs. (8–10) and (13) to a very large value [consistent with setting the plasma density n_0 to zero in Eq. (5)]. This result is shown as the dotted line in Fig. 16. It is numerically the same result that one achieves applying the well-known solution for the potential between two cylindrical electrodes in a vacuum or air:

$$\phi(r) = (\phi_a - \phi_b)\frac{\ell_n(b/r)}{\ell_n(b/a)} + \phi_b \tag{14}$$

so that the solution checks out in the limit of no plasma. We can also recover the case of the plane parallel plasma capacitor from this solution by setting the inner radius a large compared to the gap length. Setting $a = 500$, and keeping $b - a = 10$, we have the result shown in Fig. 17, for the case of plasma present (solid line) and for the case of plasma absent (dotted line). The latter case is, of course,

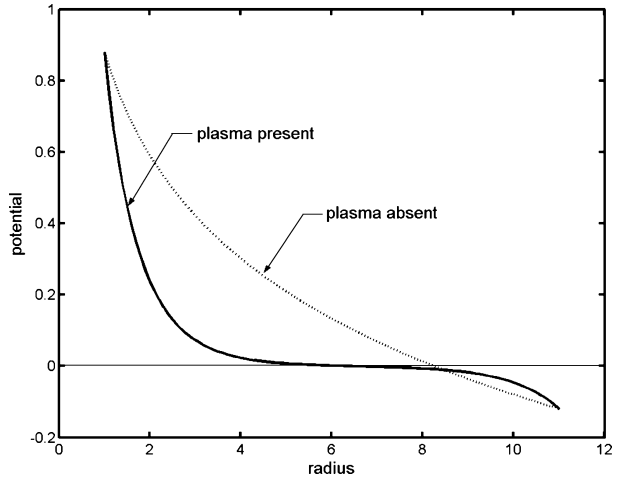

Fig. 16 Potential as a function of radius for cylindrical plasma capacitor: ——, with plasma present and · · · ·, plasma absent.

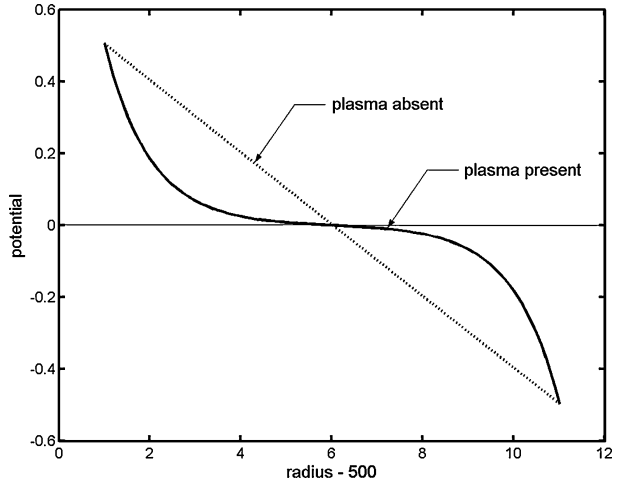

Fig. 17 In the limit of a large inner radius, cylindrical solution collapses to that of a parallel-plate capacitor: ——, plasma present or · · · ·, with uniformly decreasing potential in the gap.

a linearly decreasing potential consistent with a uniform electric field in the gap. Because this situation is geometrically symmetric, charge neutrality dictates that we set $\phi_a = 0.5$ and $\phi_b = -0.5$.

Electric Field with Asymmetric Electrodes

Because the electric field is just the gradient of the potential, and in this geometry is only in the radial direction, we can solve for the electric field in the gap by taking the derivative of Eq. (8):

$$E(r) = -\frac{\partial\phi}{\partial r} = -\frac{C_1}{\lambda_D} I_1\left(\frac{r}{\lambda_D}\right) + \frac{C_2}{\lambda_D} K_1\left(\frac{r}{\lambda_D}\right) \tag{15}$$

These results, for the same parameters as earlier, are shown in Fig. 18 (solid line). The electric field in the bulk of the plasma is effectively shielded, whereas the electric field near the boundaries is elevated, compared to the results with plasma absent (dotted line), again found by setting the Debye length in our equations to a large value. As before, the results in the absence of plasma agree numerically with the solution in vacuum or air given by

$$E(r) = [(\phi_a - \phi_b)/\ell_n(b/a)](1/r) \tag{16}$$

In the limit of large inner radius, the value of the electric field calculated using the cylindrical solution is symmetric, as shown in Fig. 19. In particular, with the plasma absent, the electric field is constant and its magnitude is equal to the potential difference

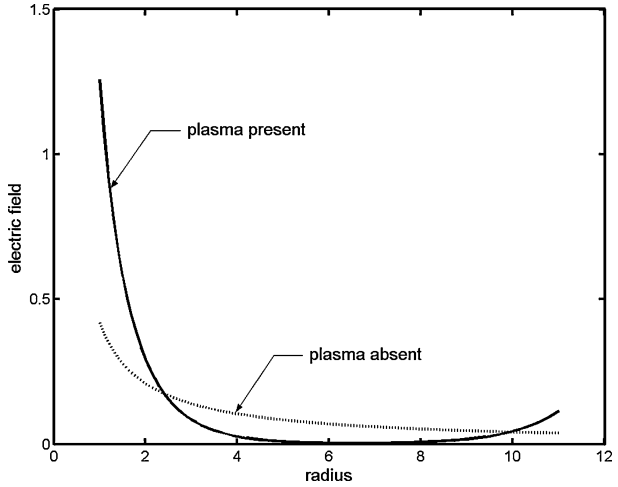

Fig. 18 Electric field, in the presence of the plasma, also shielded in bulk of the plasma; cylindrical solution agrees with vacuum solution in limit of large Debye length.

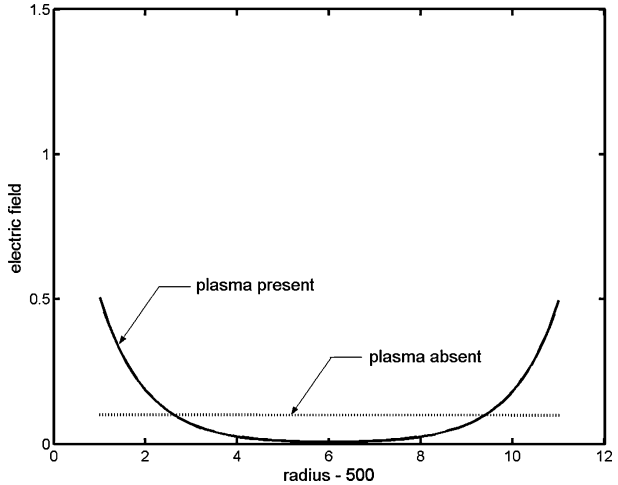

Fig. 19 Electric field given by Eq. (15) behaves as expected in limit of large inner radius; in particular, with the plasma absent, E-field in gap is uniform.

divided by the gap length, consistent with the familiar result for a parallel plate capacitor. This gives us additional confidence that the solution is indeed correct.

Electric Forces on the Plasma

Because there is an electric field in the plasma in regions where there is also a net charge density, there will be a force on the plasma. The force density (force per unit volume or body force) can be calculated directly and self-consistently by taking the electric field multiplied by the charge density. Because the charge density is proportional to the potential, however, we can write

$$\boldsymbol{f} = \rho \boldsymbol{E} = -\left(\varepsilon_0 \big/ \lambda_D^2\right)\phi \boldsymbol{E} \tag{17}$$

where we choose to use a lower-case f as a reminder that this is a volumetric quantity. In the cylindrical geometry, this force density will be in the radial direction. Because we have expressions for ϕ and E, we can write a similar expression for the radial component of $\boldsymbol{f}$:

$$\begin{aligned} f_r(r) = {} & \left(\varepsilon_0 C_1^2 \big/ \lambda_D^3\right) I_0(r/\lambda_D) I_1(r/\lambda_D) \\ & - \left(\varepsilon_0 C_1 C_2 \big/ \lambda_D^3\right) I_0(r/\lambda_D) K_1(r/\lambda_D) \\ & + \left(\varepsilon_0 C_1 C_2 \big/ \lambda_D^3\right) K_0(r/\lambda_D) I_1(r/\lambda_D) \\ & - \left(\varepsilon_0 C_2^2 \big/ \lambda_D^3\right) K_0(r/\lambda_D) K_1(r/\lambda_D) \end{aligned} \tag{18}$$

Figure 20 shows the calculation of the force density as a function of radius. The force density is concentrated near the inner conductor and is negative in sign there, that is, it is directed inward toward the electrode. One important aspect of this model is that the force is inwardly directed even if we change the polarity of the potential drop across the electrodes. This is because as the sign of the potential changes at any point in space, so does the sign of the net charge density there [by Eq. (6)], so that the direction of the force is unchanged. This result of the model is consistent with our previous experimental measurements, which demonstrate that the force on the actuator is determined by the asymmetry in the electrode geometry independent of the polarity of the applied voltage.

Finally, Fig. 20 also shows that in the limit of a large Debye length (in other words, in the absence of plasma) there is no body force. This stands to reason because, if the force depends on a charge separation in the plasma, without any charges to separate there can be no force. It has been suggested by Roth et al.[23] that because the quantity $\varepsilon_0 E^2/2$ has units of energy density the gradient of this quantity may be taken for the force density or body force. As we show in the Appendix to this paper, this expression is only an approximation. Because, in the case of the cylindrical plasma capacitor, we have an explicit, exact expression for $\boldsymbol{E}$, we can calculate the quantity $\varepsilon_0 E^2/2$ and test the validity of this approximation directly. Because the case we are considering is radially symmetric, we need only consider the radial derivative in calculating the gradient:

$$\begin{aligned} \frac{\partial}{\partial r}\frac{\varepsilon_0}{2}E^2 = {} & \frac{\varepsilon_0 C_1^2}{2\lambda_D^3} I_1\left(\frac{r}{\lambda_D}\right)\left[I_0\left(\frac{r}{\lambda_D}\right) + I_2\left(\frac{r}{\lambda_D}\right)\right] \\ & + \frac{\varepsilon_0 C_1 C_2}{2\lambda_D^3} I_1\left(\frac{r}{\lambda_D}\right)\left[K_0\left(\frac{r}{\lambda_D}\right) + K_2\left(\frac{r}{\lambda_D}\right)\right] \\ & - \frac{\varepsilon_0 C_1 C_2}{2\lambda_D^3} K_1\left(\frac{r}{\lambda_D}\right)\left[I_0\left(\frac{r}{\lambda_D}\right) + I_2\left(\frac{r}{\lambda_D}\right)\right] \\ & - \frac{\varepsilon_0 C_2^2}{2\lambda_D^3} K_1\left(\frac{r}{\lambda_D}\right)\left[K_0\left(\frac{r}{\lambda_D}\right) + K_2\left(\frac{r}{\lambda_D}\right)\right] \end{aligned} \tag{19}$$

The dotted lines in Fig. 20 are the results of the approximation expressed Eq. (19). The solid lines in Fig. 20 are the results of the exact calculation from Eq. (18). There is general agreement between the two for the case in which plasma is present, although the grad-E^2 approximation overpredicts the force density. The approximation is incorrect with the plasma absent, however, for a simple reason: Even without plasma present, there is still a spatial structure to the E field and, therefore, a gradient in E^2. Without plasma present, however, there is no charge separation and, therefore, nothing for the electric field to act upon, so that a nonzero value for the force density is an artifact. Because, to determine the effect of the plasma, it is necessary to calculate explicitly the spatial distribution of the potential, a correct approach to the problem already gives one the means to calculate readily the exact solution, rendering the grad-E^2 approximation superfluous.

Behavior Predicted from the Model

In its ability to predict the behavior of the aerodynamic plasma actuator, this abstract model of the system is successful in two instances and unsuccessful in a third. As presented in Fig. 20 and discussed in the preceding paragraphs, the model correctly predicts that force from the actuator decreases with decreasing plasma density (increasing Debye length) and that in the limit of no plasma no force exists. In practice, we measure the net force exerted by the plasma actuator, not the force density, and so we take as a figure of merit from the calculations the integral of Eq. (18) over the volume of the model. [Because the only variations in this model are in the radial direction, the sign of the result of Eq. (18) captures the vector nature of the force.] Figure 21 shows this resulting net

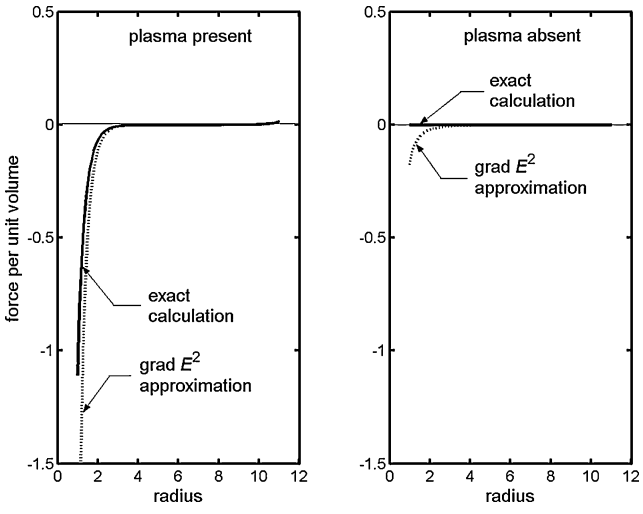

Fig. 20 In presence of plasma, there is a body force near the smaller electrode, directed toward that electrode; in the absence of plasma, there is no body force; approximating body force as the gradient of $\varepsilon_0 E^2/2$ is an especially poor approximation in the absence of plasma.

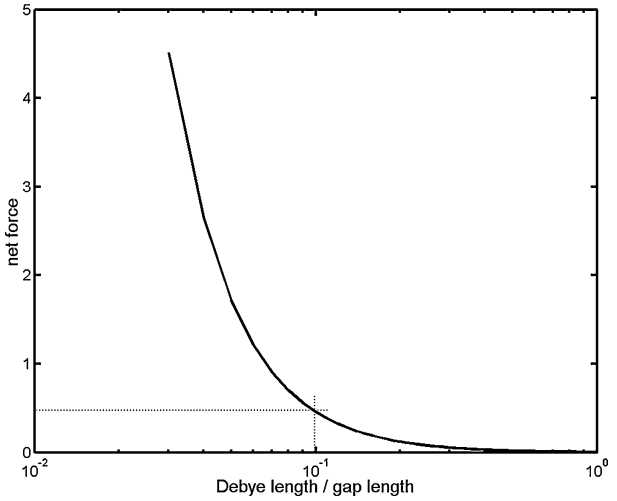

Fig. 21 Predictions of the concentric-cylinder model indicate that the greater the plasma density (equivalent to the shorter the Debye length) the greater the net thrust from the actuator.

force as a function of the Debye length. Although in the laboratory it is difficult to separate density effects from effects related to the simple magnitude of the applied field, these predictions are at least not inconsistent with the measured results. (In general, in the laboratory, the more voltage we apply to the actuator, the more plasma we get.) In particular, it is typical to have to apply several kilovolts across the actuator before the plasma ignites at all, and even with this substantial voltage, there is no measurable force with no plasma present.

Another conclusion from this model, namely, that the body force is concentrated near the edge of the exposed electrode and is directed toward the electrode at that point, is in agreement with airflows in the vicinity of the actuator measured in the laboratory and calculated numerically. We have inserted body force calculations based on realistic electrode geometries into computational fluid dynamics (CFD) codes to predict the actuator's behavior, and the results of these calculations (Fig. 22) closely match the airflows measured by proportional integral derivative techniques. Theory and measurement agree that the region downstream of the exposed electrode edge is the critical region for the actuator.

The predictions of the abstract model are at odds, however, with the unambiguous observation presented in this paper (Fig. 12) that thrust increases with decreasing radius of the exposed electrode. As Fig. 23 shows, the abstract model predicts that net thrust decreases,

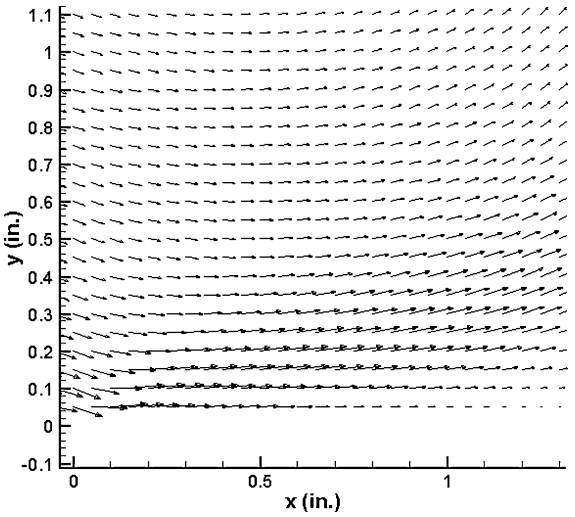

Fig. 22 CFD calculations including an electrostatic body force highly concentrated near the exposed electrode edge and inwardly directed there in substantial agreement with flows measured in laboratory.

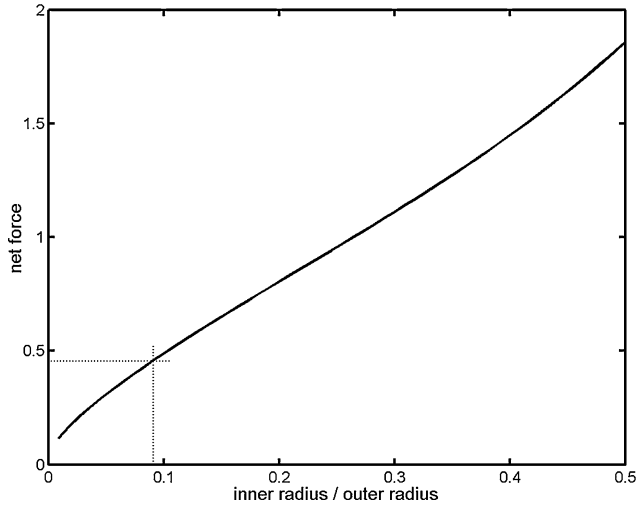

Fig. 23 Prediction of model is that thrust decreases with decreasing diameter of the smaller conductor, inconsistent with experimental results in Fig. 10.

almost linearly, as the radius of the inner conductor is reduced. It is straightforward to see why this is so in the model because our figure of merit is the force density integrated over the volume of the model. The magnitude of the calculated body force does indeed increase as the inner radius is reduced, but the volume over which this body force exists drops off more rapidly than the body force increases, so that the overall effect is that the net force is reduced. This relationship is not limited to the cylindrical geometry: We see the same behavior in the finite element solutions with the more realistic geometries. As Fig. 14 shows, the region of the largest electric field is limited to within approximately a Debye length of the exposed electrode, and as the dimension of this electrode decreases, so does the volume of this interaction region.

The shortcoming of the abstract model is that it assumes a uniform plasma density throughout the region at all times, although we know from our own measurements (Figs. 4 and 5) that this approximation is not correct at any time during the developing discharge. Also, the model treats the plasma as a stationary charged particle density, which ignores that it is created and sustained from an electrical discharge through it. This implies a more complicated sheath structure near the electrodes than is described by Eq. (6). Unfortunately, it is unlikely that a model of this fidelity can be solved in a closed form. We are currently building a numerical model to perform the required two-dimensional, time-dependent calculation of the E field and particle densities in the discharge region, which includes the electric fields within the sheath regions of the discharge near the electrodes. The results presented here imply that this tool will be necessary to predict the behavior of the plasma actuator with reasonable accuracy.

Conclusions

Charge separation within the dielectric barrier discharge plasma that forms the aerodynamic plasma actuator is a possible means through which the electric field can exert a net force on the plasma and, through subsequent interactions, to the surrounding gas. A straightforward model of the actuator predicts that the largest force density associated with this mechanism will be in a small region adjacent to the exposed electrode, and this supposition is consistent with the observed flows of neutral gas induced by the actuator. The importance of the region near the exposed electrode to the operation of the device is confirmed by measurements that demonstrate that the dimensions of the exposed electrode strongly determine the performance of the actuator, even though the bulk properties of the discharge remain unaffected. Although instructive, the static model presented here is at best a sketch of the plasma behavior. Because the actuator plasma exhibits considerable structure in space and time, a detailed two-dimensional, time-dependent calculation of the field structure with the plasma present will be necessary to predict accurately the body force imparted by the plasma on the neutral fluid. For example, such an approach is likely to reveal considerable structure in the expanding edge of the plasma, and we show here that the expansion of the plasma, which is governed in part by the geometry of the lower, insulated electrode, has as considerable an impact on the performance of the actuator as the geometry at the exposed electrode edge.

Appendix: Discussion of the grad-E^2 Approximation

The assertion by Roth et al.[23] that the body force $\boldsymbol{f}$ can be calculated from the gradient in the electric field via the equation

$$\boldsymbol{f} = (\varepsilon_0/2)\boldsymbol{\nabla} E^2 \tag{A1}$$

rests on the assertion that

$$\boldsymbol{\nabla} E^2 = 2\boldsymbol{E}(\nabla \cdot \boldsymbol{E}) \tag{A2}$$

Using this substitution in Eq. (A1) and using that the electric field is just the negative of the gradient in the potential, we have

$$\boldsymbol{f} = (\varepsilon_0/2)2\boldsymbol{E}(\boldsymbol{\nabla} \cdot \boldsymbol{E}) = -\varepsilon_0 \boldsymbol{E}(\boldsymbol{\nabla} \cdot \boldsymbol{\nabla}\phi) = -\varepsilon_0 \boldsymbol{E}\, \nabla^2\phi \tag{A3}$$

but because, by Eq. (4), the potential is related to the charge density by the relation $-\nabla^2\phi = \rho/\varepsilon_0$, Eq. (A3) is just

$$\boldsymbol{f} = -\varepsilon_0 \boldsymbol{E}\,\nabla^2\phi = -\varepsilon_0 \boldsymbol{E}(-\rho/\varepsilon_0] = \rho\,\boldsymbol{E} \tag{A4}$$

in agreement with Eq. (17). The validity of Eq. (A1), then, rests on the validity of Eq. (A2). In general, however, Eq. (A2) is only an approximation. It is straightforward to show in three dimensions (so that $\boldsymbol{E} = E_x\hat{i} + E_y\hat{j} + E_z\hat{k}$) that

$$\begin{aligned}
\nabla E^2 &= \frac{\partial E^2}{\partial x}\hat{i} + \frac{\partial E^2}{\partial y}\hat{j} + \frac{\partial E^2}{\partial z}\hat{k} = \frac{\partial}{\partial x}\left(E_x^2 + E_y^2 + E_z^2\right)\hat{i} \\
&+ \frac{\partial}{\partial y}\left(E_x^2 + E_y^2 + E_z^2\right)\hat{j} + \frac{\partial}{\partial z}\left(E_x^2 + E_y^2 + E_z^2\right)\hat{k} \\
&= \left(2E_x\frac{\partial E_x}{\partial x} + 2E_y\frac{\partial E_y}{\partial x} + 2E_z\frac{\partial E_z}{\partial x}\right)\hat{i} \\
&+ \left(2E_x\frac{\partial E_x}{\partial y} + 2E_y\frac{\partial E_y}{\partial y} + 2E_z\frac{\partial E_z}{\partial y}\right)\hat{j} \\
&+ \left(2E_x\frac{\partial E_x}{\partial z} + 2E_y\frac{\partial E_y}{\partial z} + 2E_z\frac{\partial E_z}{\partial z}\right)\hat{k}
\end{aligned} \tag{A5}$$

whereas

$$\begin{aligned}
2\boldsymbol{E}(\nabla\cdot\boldsymbol{E}) &= 2(E_x\hat{i} + E_y\hat{j} + E_z\hat{k})\left(\frac{\partial E_x}{\partial x} + \frac{\partial E_y}{\partial y} + \frac{\partial E_z}{\partial z}\right) \\
&= 2E_x\left(\frac{\partial E_x}{\partial x} + \frac{\partial E_y}{\partial y} + \frac{\partial E_z}{\partial z}\right)\hat{i} \\
&+ 2E_y\left(\frac{\partial E_x}{\partial x} + \frac{\partial E_y}{\partial y} + \frac{\partial E_z}{\partial z}\right)\hat{j} \\
&+ 2E_z\left(\frac{\partial E_x}{\partial x} + \frac{\partial E_y}{\partial y} + \frac{\partial E_z}{\partial z}\right)\hat{k}
\end{aligned} \tag{A6}$$

In general, we see that the right-hand sides of Eqs. (A5) and (A6) are not equal to each other. There is one case in which these two give the same result, namely, the strictly one-dimensional case in which $\boldsymbol{E} = E_x\,\hat{i}$ and $E_y = E_z = 0$, and $\partial/\partial y = \partial/\partial z = 0$ as well. In this limited case, Eq. (A2) holds. As we have already shown in this paper, however, this is the well-known case of the one-dimensional plasma capacitor. As Figs. 14 and 16 show, due to the symmetry of the problem, there can be no net force generated on the plasma in the one-dimensional case regardless of how much plasma is in the gap. The one case, therefore, in which the grad-E^2 approximation strictly applies is the one case that does not apply to the aerodynamic plasma actuator.

Acknowledgment

The authors gratefully acknowledge the support of the Air Force Research Laboratory (AFRL) Munitions Directorate, AFRL/MNAV, Eglin Air Force Base, Florida, in conducting this research.

References

[1]Kogelschatz, U., "Filamentary, Patterned, and Diffuse Barrier Discharges," *IEEE Transactions on Plasma Science*, Vol. 30, 2002, p. 1400.

[2]Haacke, M., Humpert, C., and Pietsch, G. J., "Influence of Field Strength and Energy Distribution of Different Barrier Discharge Arrangements on Ozone Generation," *Ozone Science and Engineering*, Vol. 24, 2002, pp. 193–201.

[3]Mangolini, L., Orlov, K., Kortshagen, U., Heberlein, J., and Kogelschatz, U., "Study of Different Discharge Regimes in a Dielectric Barrier Discharge: Electrical and Optical Characterization," American Physical Society, 55th Annual Gaseous Electronics Conf., Paper NR2.003, Oct. 2002.

[4]Kang, W. S., Kim, Y., and Hong, S. E., "Spatio-Temporal Images of Single Streamer Propagation in Dielectric Barrier Discharge," *IEEE Transactions on Plasma Science*, Vol. 30, 2002, pp. 166, 167.

[5]Napatovich, A. P., "Overview of Atmospheric Pressure Discharges Producing Nonthermal Plasma," *Plasmas and Polymers*, Vol. 6, No. 1, 2001, pp. 1–14.

[6]Gherardi, N., and Massines, F., "Mechanisms Controlling the Transition from Glow Silent Discharge to Streamer Discharge in Nitrogen," *IEEE Transactions on Plasma Science*, Vol. 29, 2001, pp. 536–544.

[7]Liu, S., and Neiger, M., "Excitation of Dielectric Barrier Discharges by Unipolar Submicrosecond Square Pulses," *Journal of Physics D: Applied Physics*, Vol. 34, 2001, pp. 1632–1638.

[8]Kunhardt, E. E., "Generation of Large-Volume, Atmospheric-Pressure, Nonequilibrium Plasmas," *IEEE Transactions on Plasma Science*, Vol. 28, 2000, pp. 189–200.

[9]Gibalov, V. I., and Pietsch, G. J., "The Development of Dielectric Barrier Discharges in Gas Gaps and on Surfaces," *Journal of Physics D: Applied Physics*, Vol. 33, 2000, pp. 2618–2636.

[10]Steinle, G., Neundorf, D., Hiller, W., and Pietralla, M., "Two-Dimensional Simulation of Filaments in Barrier Discharges," *Journal of Physics D: Applied Physics*, Vol. 32, 1999, pp. 1350–1356.

[11]Massines, F., Rabehi, A., Decomps, P., Ben Gadri, R., Segur, P., and Mayoux, C., "Experimental and Theoretical Study of a Glow Discharge at Atmospheric Pressure Controlled by Dielectric Barrier," *Journal of Applied Physics*, Vol. 83, 1998, pp. 2950–2957.

[12]Xu, X., and Kushner, M. J., "Multiple Microdischarge Dynamics in Dielectric Barrier Discharges," *Journal of Applied Physics*, Vol. 84, 1998, pp. 4153–4160.

[13]Li, J., and Dhali, S. K., "Simulation of Microdischarges in a Dielectric-Barrier Discharge," *Journal of Applied Physics*, Vol. 82, 1997, pp. 4205–4210.

[14]Falkenstein, Z., and Coogan, J. J., "Microdischarge Behavior in the Silent Discharge of Nitrogen–Oxygen and Water–Air Mixtures," *Journal of Physics D: Applied Physics*, Vol. 30, 1997, pp. 817–825.

[15]Enloe, C. L., McLaughlin, T. E., VanDyken, R. D., Kachner, K. D., Jumper, E. J., and Corke, T. C., "Mechanisms and Responses of a Single Dielectric Barrier Plasma Actuator: Plasma Morphology," *AIAA Journal*, Vol. 42, No. 3, 2004, pp. 589–594.

[16]Enloe, C. L., McLaughlin, T. E., VanDyken, R. D., Kachner, K. D., Jumper, E. J., and Corke, T. C., "Mechanisms and Responses of a Single Dielectric Barrier Plasma," AIAA Paper 2003-1021, Jan. 2003.

[17]Wilkinson, S., "Investigation of an Oscillating Surface Plasma for Turbulent Drag Reduction," AIAA Paper 2003-1023, Jan. 2003.

[18]Post, M., and Corke, T., "Separation Control on High Angle of Attack Airfoil Using Plasma Actuators," AIAA Paper 2003-1024, Jan. 2003.

[19]Ashpis, D., and Hultgren, L., "Demonstration of Separation Delay with Glow Discharge Plasma Actuators," AIAA Paper 2003-1025, Jan. 2003.

[20]List, J., Byerley, A., McLaughlin, T., and VanDyken, R., "Using Plasma Actuator Flaps to Control Laminar Separation on Turbine Blades in a Linear Cascade," AIAA Paper 2003-1026, Jan. 2003.

[21]Huang, J., Corke, T., and Thomas, F., "Plasma Actuators for Separation Control of Low Pressure Turbine Blades," AIAA Paper 2003-1027, Jan. 2003.

[22]Corke, T. C., Jumper, E. J., Post, M. L., Orlov, D., and McLaughlin, T. E., "Application of Weakly-Ionized Plasmas as Wing Flow-Control Devices," AIAA Paper 2002-0350, Jan. 2002.

[23]Roth, J. R., and Sherman, D. M., "Electrohydrodynamic Flow Control with a Glow-Discharge Surface Plasma," *AIAA Journal*, Vol. 38, 2000, pp. 1166–1172.

[24]Corke, T. C., and Matlis, E., "Phased Plasma Arrays for Unsteady Flow Control," AIAA Paper 2000-2323, Jan. 2000.

[25]Roth, J. R., Sherman, D. M., and Wilkinson, S. P., "Boundary Layer Flow Control with A One Atmosphere Uniform Glow Discharge Surface Plasma," AIAA Paper 98-0328, Jan. 1998.

[26]Enloe, C. L., "Optical and Electrical Measurements of a Highly Asymmetric Dielectric Barrier Discharge for Flow Control on Aerodynamic Surfaces," American Physical Society, 55th Annual Gaseous Electronics Conf., Paper QWP 87, Oct. 2002.

[27]Vidmar, R. J., and Stalder, K. R., "Air Chemistry and Power to Generate and Sustain Plasma: Plasma Lifetime Calculations," AIAA Paper 2003-1189, Jan. 2003.

[28]Jackson, J. D., *Classical Electrodynamics*, 2nd ed., Wiley, New York, 1975, pp. 75–78.

[29]Chen, F. F., *Introduction to Plasma Physics and Controlled Fusion, Volume 1: Plasma Physics*, 2nd ed., Plenum, New York, 1984, pp. 8–11.

[30]Krall, N. A., and Trivelpiece, A. W., *Principles of Plasma Physics*, San Francisco Press, San Francisco, 1986, pp. 4, 72, 73.

[31]FEMLAB, Ver. 2.3a, Comsol, Inc., Burlington, MA, April 2003.

J. Gore
Associate Editor